JOURNAL OF CATALYSIS 142, 274–288 (1993)

Reduction and Sulfidation Properties of Iron Species in Iron-Supported Y-Zeolite by Temperature-Programmed Reduction and Sulfiding

KAZUHIRO INAMURA, RYUICHIRO IWAMOTO, AKIRA IINO, AND TOSHIYUKI TAKYU

Central Research Laboratories, Idemitsu Kosan Co., Ltd., 1280 Kamiizumi, Sodegaura, Chiba 299-02, Japan

Received November 2, 1992; revised February 19, 1993

Temperature-programmed reduction (TPR) and temperature-programmed sulfiding (TPS) were used to characterize reduction and sulfiding properties of Fe-exchanged Y-zeolites and Fe-treated Y-zeolites, which were prepared by treating NH_4Y-zeolite with an aqueous ferric nitrate solution (Fe-treatment). By considering their unique TPR and TPS patterns, it was confirmed that the Fe^{2+}-species in the Fe-exchanged Y-zeolites are stabilized inside the sodalite cages and the hexagonal prisms. On the basis of the TPR and TPS characterizations, it was demonstrated that three types of the Fe-species are present in the Fe-treated Y-zeolites: ion-exchanged species, small Fe oxide clusters, and Fe oxide without interaction with the zeolite framework (including aggregated ferric oxide), the proportion of which is dependent on the extent of the Fe-treatment. Prolonged Fe-treatment weakens the interaction between the Fe-species and the framework oxygen atoms by hydrolysis, and leads to the aggregation of the Fe oxides and to the formation of bulk ferric oxide. The small Fe-oxide clusters, which are probably situated inside the supercages through a coordination with the framework oxygen atoms, are responsible for the high activity for toluene disproportionation in the presence of H_2S.

INTRODUCTION

Zeolite catalysts are widely used for important industrial petroleum processes such as fluid catalytic cracking (FCC), hydrocracking (HYC), isomerization, and dewaxing. In the recent decade, Idemitsu Kosan Co., Ltd. has been developing resid hydrocracking catalysts, which contain modified Y-zeolites, for hydrocracking atmospheric residual oil in a fixed bed process. Especially the catalysts containing Fe-treated Y-zeolites, which were obtained by treating Y-zeolites with an aqueous solution of $Fe(NO_3)_3$, showed both high hydrocracking activity and high selectivity to middle distillates (*1*). One of the typical Fe-treated Y-zeolites (FeHY-1), prepared from NH_4Y (LZY-82), exhibited high activity and low coke deposition for toluene disproportionation in a flow of H_2S/H_2 (*2, 3*). Detailed investigation of FeHY-1 by means of ESR, FT-IR, transmission electron microscope (TEM) (*4, 5*), and Mössbauer spectroscopy (*5, 6*) has shown the presence of superfine ferric oxide (particle size <1 nm), which strongly interacts with the zeolite framework. Although a study of the nature of the iron species in the catalyst has been made, the mechanism of formation of the active species has remained obscure. Furthermore, a quantitative determination of the active species was urgently required for the production control of the commercial Fe-treated Y-zeolite catalysts.

Most studies of iron-containing Y-zeolite catalysts have concentrated on Fe-exchanged Y-zeolites (Fe–Y) (*7–13*). Boudart and co-workers reported the reversible oxidation–reduction ($Fe^{2+} \rightleftharpoons Fe^{3+}$) of Fe ions exchanged into Y-zeolite (*7, 8*). The redox properties of Fe–Y were applied in the catalytic decomposition of N_2O by Hall and coworkers (*10–12*). They reported that the silicon-substituted Fe–Y catalysts had higher turnover frequencies for the decomposition

0021-9517/93 $5.00

of N_2O than the conventional Fe–Y catalyst (Si/Al molar ratio = 2.47) (*12*). More recently, the Si/Al ratio was confirmed to have a significant effect on the distribution of the Fe cations in accessible (I′, II′, and/or II) and inaccessible (I) sites of the zeolite (*13*). These results suggest that the catalytic and redox properties of Fe–Y are strongly associated with the location of the Fe ions in the zeolite pores and with the state of the Fe ions. Consequently, investigation of the redox properties of these catalysts might provide structural information about the iron–zeolite interaction. Moreover, the sulfidation properties of the catalysts could also give useful information, since FeHY-1 showed high activity for toluene disproportionation in the presence of H_2S (*2*).

The objective of this study was to examine the details of the reduction and sulfidation properties of Fe-supported Y-zeolites, which included both Fe-exchanged and Fe-treated Y-zeolites, by using temperature-programmed reduction (TPR) and temperature-programmed sulfiding (TPS). A series of Fe-treated Y-zeolites, which were collected during the preparation process of FeHY-1, as well as two well characterized Fe-exchanged Y-zeolites, were examined. Investigations of the influences of preparation conditions on physicochemical properties and catalytic activities of Fe-treated Y-zeolites have been reported (*2, 3*). In this paper, the reduction/sulfidation properties and the active Fe-species are elucidated and an interpretation of the reduction and sulfidation mechanisms of Fe-supported Y-zeolites is presented.

EXPERIMENTAL

Catalyst Preparation

Two Fe-exchanged Y-zeolites were prepared by treating two types of NH_4Y-zeolites (Linde: SK-41; UCC: LZY-82) with an aqueous solution of $FeSO_4$ (0.25 *M*, 333 K, 60 min) under a nitrogen atmosphere, according to the procedure reported by Boudart and co-workers (*7*). After exchanging three times with ferrous ions, the zeolites

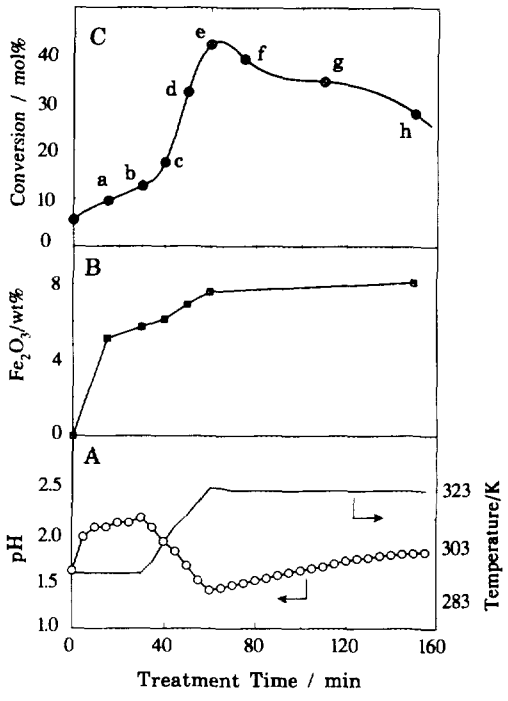

FIG. 1. The change in physicochemical properties of Fe/LZY(a)–(h) as a function of treatment time: (A) pH (left) and temperature (right) of the zeolite suspension, (B) the amount of supported iron (as Fe_2O_3) on the zeolite, and (C) catalytic activity for toluene disproportionation.

were filtered and washed with hot distilled-deionized water, and dried at room temperature *in vacuo* overnight. The Fe-exchanged Y-zeolites obtained by treating SK-41 and LZY-82 are denoted Fe–SK and Fe–LZY, respectively. In addition, Fe–LZY(A), which has been reported as "FeHY-2" in our previous report (*2*), was prepared by treating LZY-82 with an aqueous solution of $FeSO_4$ (1 *M*, 363 K, 120 min) in air.

On the basis of the preparation procedure for FeHY-1 (*2, 3*), a series of Fe-treated Y-zeolites was prepared by treating LZY-82 with a 0.250 *M* $Fe(NO_3)_3$ solution at room temperature, followed by heating to 323 K. Subsequently, the temperature of the zeolite suspension was kept at 323 K for 2 h (see Fig. 1A). Part of the suspension was filtered at 10–30 min intervals, washed with hot dis-

TABLE 1

Preparation Conditions for Fe-Exchanged and Fe-Treated Y-Zeolites

Catalyst	Fe solution		Fe soln./Y[a] (ml g^{-1})	Treating conditions		
	Salt	Conc[b] (*M*)		Temp	Time	Atmosphere
Fe–SK	$FeSO_4$	0.25	20	333 K	60 min[c]	N_2
Fe–LZY	$FeSO_4$	0.25	20	333 K	60 min[c]	N_2
Fe–LZY(A)[d]	$FeSO_4$	1.00	40	363 K	120 min	Air
Fe/LZY(a)–(i)[e]	$Fe(NO_3)_3$	0.25	8	293–323 K	15–150 min	Air
FeHY-1	$Fe(NO_3)_3$	0.25	8	323 K	120 min	Air

[a] Ratio of the volume (ml) of the aqueous iron salt solution to the amount (g) of the zeolite powder.
[b] Concentration of the iron salt in the aqueous solution.
[c] Fe-exchange treatment was repeated three times.
[d] Fe–LZY(A) was referred to as FeHY-2 in Ref. (*2*).
[e] Detailed preparation conditions are shown in the text and in Fig. 1. Fe/LZY(i) was obtained from the residual slurry after cooling down to room temperature overnight.

tilled water, and dried at 363 K for 3 h in static air. The resulting Fe-treated Y-zeolites are denoted Fe/LZY(a)–(h) depending on the sampling time, as shown in Fig. 1C. Fe/LZY(i) was obtained from the residual slurry after cooling down to room temperature overnight.

The preparation conditions for Fe-exchanged and Fe-treated Y-zeolites are summarized in Table 1. Variations of the physicochemical properties during the preparation process of FeHY-1 are shown in Fig. 1. The amounts of iron in the catalysts, as well as the Si/Al molar ratios of the catalysts, were measured with an X-ray fluorescence spectrometer (XRF). The crystallinity of the sample was determined by X-ray diffraction (XRD) employing Cu$K\alpha$ radiation with an Ni filter. The unit cell parameters of the zeolite framework were determined from the average 2θ values of the (642) and (555) peaks of the zeolite crystal, which were corrected for the 2θ value of Si(111) as 28.443° with an Si crystal (99.999%) as internal standard. Solid-state ^{29}Si NMR spectra were recorded on a JEOL GX-270 FT-NMR equipped with a magic angle spinning accessory, operating at a resonance frequency of 53.55 MHz. Prior to NMR measurements, all samples were equilibrated with water vapor in a desiccator containing saturated $CaCl_2 \cdot 6H_2O$, in order to avoid the spectral broadening for dehydrated faujasites (*14*). The amount of supported iron species, the Si/Al molar ratio (XRF and NMR), and the unit cell parameter of the samples are listed in Table 2.

TABLE 2

Chemical Properties of Fe-Exchanged and Fe-Treated Y-Zeolites

Catalyst	Fe_2O_3[a] (wt%)	Si/Al ratio		a_0[c] (nm)
		XRF	NMR[b]	
SK-41	Traces	2.55	2.6	2.473
Fe–SK	12.5	2.5	—	2.470
LZY-82	Traces	2.92	4.8	2.457
Fe–LZY	5.3	3.0	—	2.451
Fe–LZY(A) (FeHY-2)	11.8	3.1	—	2.451
Fe/LZY(b)	5.7	3.4	—	2.445
Fe/LZY(h)	8.2	5.4	—	2.442
Fe/LZY(i)	9.9	5.4	—	2.439
FeHY-1	9.0	5.3	—	2.440

[a] Amount of supported iron as Fe_2O_3 measured by X-ray fluorescence (XRF).
[b] Si/Al molar ratio in zeolite framework determined by ^{29}Si MAS NMR.
[c] Unit cell parameter of zeolite framework determined by X-ray diffraction (XRD).

Catalytic Reaction

The activities of toluene disproportionation were measured with a high pressure continuous flow micro reactor. Toluene was fed at rate of 10 $cm^3\ h^{-1}$ in a flow of 0.2 vol% H_2S/H_2 (200 $cm^3\ min^{-1}$) under 6 MPa at 623 K. Other details on the activity measurements have been described elsewhere (*2*).

Temperature-Programmed Reduction (TPR) and Sulfiding (TPS)

The instruments and the experimental procedures for TPR and TPS have been described in detail elsewhere (*15*, *16*). The amount of catalyst used varied between 80 and 200 mg, dependent on the amount of iron in the catalyst. In the case of Fe/LZY(a)–(i), the amount was maintained at 110 mg. Before the TPR and TPS experiments, all catalysts were calcined *in situ* at 650 K for 2 h in flowing dry air (30 $cm^3\ min^{-1}$). After calcination, the catalysts were cooled to 300 K in the air and kept in flowing pure Ar (20 $cm^3\ min^{-1}$) at 300 K for more than 60 min. Thereafter the Ar flow was replaced with reacting gases [64.5% H_2/Ar (20 $cm^3\ min^{-1}$) in TPR, and mixing streams of 64.5% H_2/Ar (5.00 $cm^3\ min^{-1}$) and 5.44% H_2S/Ar (9.42 $cm^3\ min^{-1}$) in TPS, respectively] at 300 K for 90 min. Subsequently, the temperature was increased to the desired values (max 1350 K) at a constant heating rate, β, of 10 K min^{-1}. The air was dried by passage through a moisture purifier (GL Science Inc., Gas Clean Filter), while pure Ar and 64.5% H_2/Ar were purified by passage through both a moisture purifier and an oxygen purifier.

The H_2 consumption was determined with a thermal conductivity detector (TCD; Ohkura Riken Co., Ltd.) in both TPR and TPS, and the H_2S concentration in the reactant gases was analyzed with a UV spectrophotometer (Japan Spectroscopic Co., Ltd., 875-UV, set at 212 nm) in TPS. In the TPR chart positive peaks indicate H_2 consumption, whereas negative peaks show H_2 and H_2S consumption in the TPS chart.

RESULTS

Physicochemical Properties and Catalytic Activity

The variations of the physicochemical properties and catalytic activities for the samples during a treatment of FeHY-1 are shown in Fig. 1. As the same observations have already been presented in Figs. 1 and 2 in Ref. (*2*), only some distinguished properties of this series of Fe-treated Y-zeolites are briefly described. The preparation process can be divided into three stages: suspending of the Y-zeolite (LZY-82) in an $Fe(NO_3)_3$ solution at room temperature, heating the suspension to 323 K, followed by isothermal treatment at 323 K. During the first stage, the amount of supported iron increases to 5–6 wt% Fe_2O_3 after 30 min stirring of the suspension at room temperature [Fe/LZY(b)]. Nevertheless, the toluene disproportionation activity does not increase significantly compared with that of the original LZY-82. In the second stage, as the temperature of the suspension is raised from room temperature to 323 K, the activity of the resulting catalyst increases sharply to reach its highest value, while the amount of supported iron increases slightly to 7.6 wt% [Fe/LZY(e)]. The subsequent isothermal treatment in the third stage brings about a gradual decrease in the activity, while the amount of iron stays nearly constant [Fe/LZY(e)–(h)]. Throughout all stages, the Si/Al molar ratio (by XRF) increases steadily from 2.9 to 5.4 with treatment time and the crystallinity of the Y-zeolite structure decreases about 50% (*2*). As shown in Table 2, leaving the residual zeolite slurry at room temperature overnight results in an apparent increase in the amount of iron to 9.9 wt%, while the zeolite framework does not change much [Fe/LZY(i)]. Further details of physicochemical properties and catalytic activity are given in Refs. (*2*, *3*).

TPR and TPS of Fe-Exchanged Y-Zeolite

Figure 2 shows the TPR patterns of three different Fe-exchanged Y-zeolites calcined

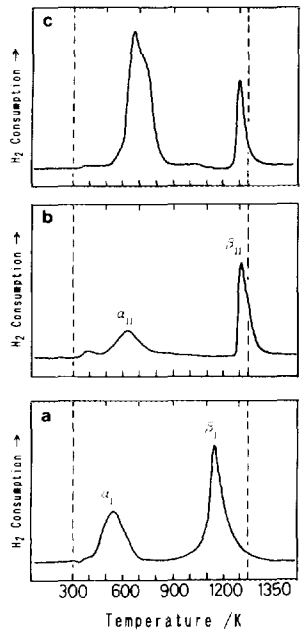

FIG. 2. TPR patterns of Fe-exchanged Y-zeolites: (a) Fe–SK, (b) Fe–LZY, and (c) Fe–LZY(A).

at 650 K for 2 h in flowing air. In a separate TPR experiment, bulk Fe_2O_3 (Rare Metallic Co., Ltd., 99.999%) was reduced completely to metal with an asymmetric peak around 720 K, in conformity with results reported by Wimmers *et al.* (*17*). The TPR patterns of the Fe-exchanged Y-zeolites such as Fe–SK and Fe–LZY are composed of two well-separated reduction peaks at low temperature (α peak) and high temperature (β peak). Fe-LZY(A) also gives two well-separated peaks, but its α peak is much larger than that of Fe–LZY, although its β peak shows the same profile and position as that of Fe–LZY.

Quantitative TPR analysis of Fig. 2 demonstrates clearly that all iron in the three samples is reduced from Fe^{3+} to metallic Fe under the TPR conditions (T_{max}: 1350 K, holding time at T_{max}: 60 min). In the case of Fe–SK and Fe–LZY, the H_2-consumption ratios of the β to α peaks ($[\beta]/[\alpha]$) are estimated to 2.0, while the reduction temperatures of Fe–LZY (α_{II}: 626 K, β_{II}: 1298 K) are appreciably higher than those of Fe–SK (α_I: 578 K, β_I: 1154 K), especially for the β peak. The H_2 consumption of the α peak for Fe–LZY(A), however, is much larger than that of the β peak (about 70% to the total H_2 consumption), and it can be decomposed into two peaks, a main peak at 652 K and a shoulder at 724 K. The temperature of the latter is in fair agreement with that of reduction of bulk Fe_2O_3, suggesting that Fe–LZY(A) contains a significant amount of aggregated ferric oxide, probably deposited on the external surface of the zeolite.

In order to elucidate what is occurring with the structure of the supported Fe and the zeolite crystal during the TPR treatment, X-ray diffraction (XRD) measurements for Fe–SK and Fe–LZY were conducted after reduction treatment at appropriate temperatures (T_{red}) between 300 and 1350 K in TPR (β: 10 K min^{-1}, holding time at T_{red}: 30 min). No diffraction peaks corresponding to Fe compounds (Fe_2O_3, metallic Fe, etc.) were detected for any sample. Figure 3 shows the

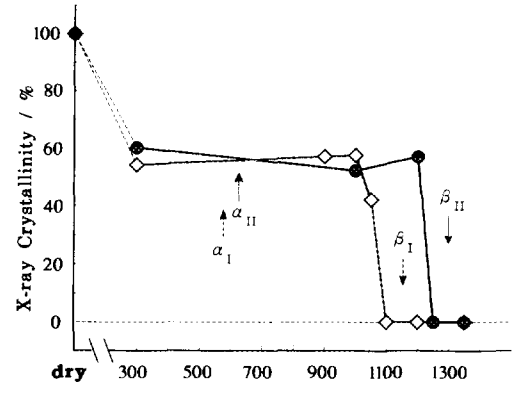

FIG. 3. X-ray crystallinity of Fe-exchanged Y-zeolite as a function of reduction temperature in TPR: (◇) Fe–SK and (●) Fe–LZY. Before TPR treatment, the catalyst was calcined at 650 K for 2 h in flowing air, except for the dried sample. The reduction temperature at 300 K in this figure signifies only calcination treatment without any reduction. The symbols $\alpha_{I,II}$ and $\beta_{I,II}$ show the peak temperatures of the α and β peaks, respectively, for Fe–SK (suffix I) and Fe–LZY (suffix II).

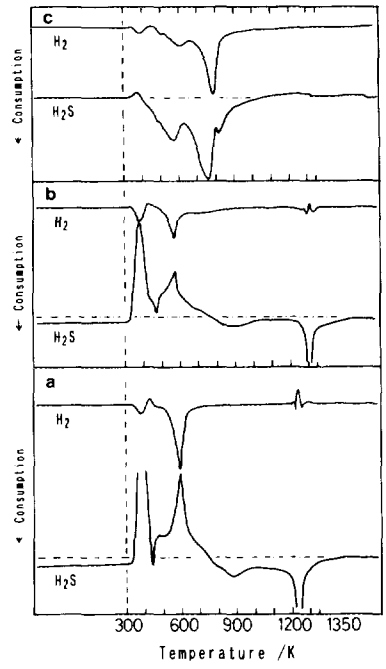

FIG. 4. TPS patterns of Fe-exchanged Y-zeolites: (a) Fe–SK, (b) Fe–LZY, and (c) unsupported Fe_2O_3 as a reference compound.

effect of reduction temperature on the X-ray crystallinity of the zeolite framework, which is defined as the ratio of the sum of the six intensive diffraction heights due to Y-zeolite [(331), (511), (440), (533), (642), and (555)] of the reduced sample against that of the original dried sample. For both Fe-exchanged Y-zeolites, a calcination treatment at 650 K in air resulted in a decrease of about 40% in the X-ray crystallinity. However, the following reduction treatment did not change the X-ray crystallinity up to the reduction temperature at ca. 1000 K for Fe–SK and at ca. 1200 K for Fe–LZY. As the reduction temperature is increased beyond this critical temperature, the X-ray crystallinity decreases abruptly to zero.

The TPS patterns of two Fe-exchanged Y-zeolites and bulk Fe_2O_3 are shown in Fig. 4. In a similar manner as the TPR results, the TPS patterns show that the sulfidation processes of the Fe-exchanged Y-zeolites are different from that of bulk Fe_2O_3. For bulk Fe_2O_3, an H_2S consumption emerges at ca. 400 K and lasts up to ca. 1000 K, accompanied by an H_2 consumption with slight retardation (or at higher temperature). The final product after TPS at 1350 K has been identified as FeS (troilite) by XRD (*16*). On the other hand, the Fe-exchanged Y-zeolites are sulfided mainly in three temperature regions: (I) a slow adsorption of H_2S during the isothermal period at 300 K, and a subsequent H_2S-evolution peak at 380 K for both Fe–SK and Fe–LZY; (II) a set of an H_2S-evolution and an H_2-consumption peak at 608 K for Fe–SK and at 586 K for Fe–LZY; and (III) a sharp and strong H_2S-consumption peak at 1225 K for Fe–SK and at 1310 K for Fe–LZY. Since the H_2S-evolution peak in region I (peak I) is also observed in the TPS pattern of the original Y-zeolite (see Fig. 7), peak I can be assigned to a desorption of weakly adsorbed H_2S molecules on the zeolite. The simultaneous appearance of the H_2S evolution and the H_2 consumption in region II (peak II) is considered to be due to the following hydrogenative desorption of adsorbed sulfur atoms on the catalyst:

$$S_{\text{on cat}} + H_2 \rightarrow H_2S. \qquad (1)$$

Similar hydrogenative desorption of sulfur has been observed in the TPS of MoO_3/Al_2O_3 (*18*) and CrO_3/Al_2O_3 (*19*). This phenomenon is observed when the metal oxide particles are so small that the substitution reaction of a metal-O to a metal-S bond already proceeds at the first stage of sulfidation. The excess sulfur should be removed by hydrogenation at higher sulfidation temperature, mainly because the ion radius of S^{2-} is much bigger than that of O^{2-}. As the H_2 consumption in peak III is negligibly small, in region III apparently only H_2S consumption occurs.

In order to obtain further information about the sulfidation mechanism of Fe-exchanged Y-zeolites, a second TPS experiment was conducted subsequently to a first TPS treatment for Fe–SK. After temperature-programmed sulfidation up to 650 K,

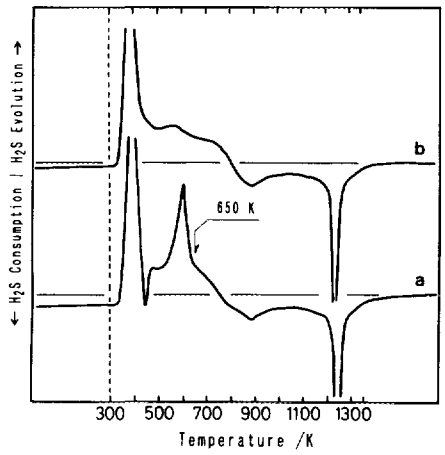

FIG. 5. TPS patterns (H_2S) of Fe–SK: (a) normal TPS pattern (the same pattern has already shown in Fig. 4a) and (b) second TPS pattern after first sulfidation at 650 K for 1 h.

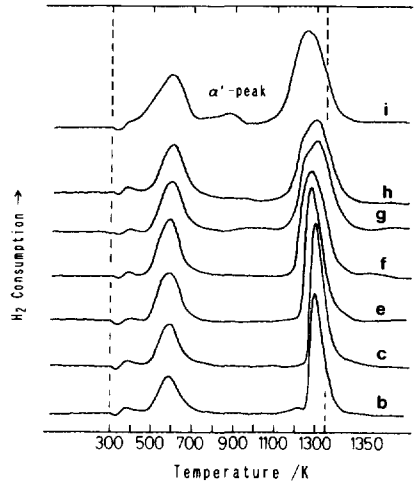

FIG. 6. TPR patterns of a series of Fe-treated Y-zeolites [Fe/LZY(b)–(i)].

followed by isothermal sulfidation at 650 K for 1 h and cooling down to room temperature under the sulfiding gases, the second TPS was run. After the TPS treatment up to and at 650 K, peak I and peak III are unchanged, but peak II has disappeared as shown in Fig. 5b. Similarly, the TPS pattern of Fe–SK after the TPR (H_2/Ar) treatment up to and at 650 K for 1 h comprises only peak I and peak III. Apparently, a sulfidation treatment at 650 K has the same effect on the successive TPS patterns of the Fe-exchanged Y-zeolite as a reduction treatment at 650 K.

TPR and TPS of Fe-Treated Y-Zeolite

The TPR and TPS (H_2S) patterns for a series of Fe-treated Y-zeolites [Fe/LZY(b)–(i)] are presented in Figs. 6 and 7, respectively. In the beginning of the Fe-treatment [Fe/LZY(b), Fe/LZY(c)], the TPR patterns are identical to that of the Fe-exchanged Y-zeolite (Fe-LZY in Fig. 2b). However, the high-temperature reduction peak (β peak) gradually broadens and shifts to lower temperature after the subsequent heat treatment, without any detectable change in the shape and position of the low-temperature reduction peak (α peak). It is noteworthy that the H_2-consumption ratio of the β to α peaks stays constant at 2.0 ($\pm$0.1) throughout the whole preparation

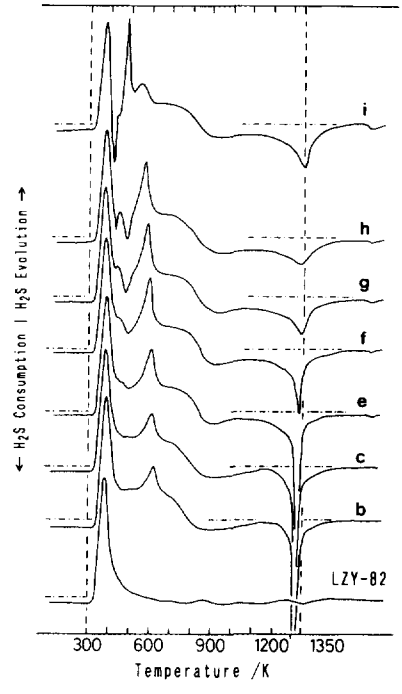

FIG. 7. TPS patterns (H_2S) of LZY-82 and a series of Fe-treated Y-zeolites [Fe/LZY(b)–(i)].

process [Fe/LZY(b)–(h)]. With Fe/LZY(i), a broad β peak appears at around 1263 K and a new reduction peak between the α and β peaks is discernible around 890 K (denoted α' peak).

It is obvious from the TPS patterns in Fig. 7 that peak I of all samples does not change in shape and position but decreases about 20% in intensity with Fe-treatment, compared with that of the original LZY-82. On the other hand, peak II and peak III show distinct changes with Fe-treatment, suggesting that these peaks may reflect some structural change in the supported iron species as well as in the zeolite framework. In the process of the Fe-treatment, the second H_2S-evolution peak (peak II) accompanied by the H_2-consumption peak synchronously shifts from 627 K [Fe/LZY(b)] to 584 K [Fe/LZY(h)] and increases in intensity. At the first stage of the treatment [Fe/LZY(b)], peak III appears at 1310 K in agreement with that of Fe-LZY, and decreases significantly in intensity, while shifting to slightly higher temperature with Fe-treatment. On the contrary, a broad H_2S consumption at 800–1200 K increases in intensity in place of peak III. The TPS pattern of Fe/LZY(i) can be differentiated from that of the others especially in terms of peak II. It shows two well-separated H_2S-evolution peaks in region II: a sharp and strong peak at 497 K, and a broader and smaller peak at 557 K, while a sharp H_2S-consumption peak appears between peak I and peak II at 415 K. The twin H_2S-evolution peaks of Fe/LZY(i) can also be classified as region II peaks, which appear as a result of reaction (1), because twin H_2-consumption peaks are observed synchronously with the H_2S evolutions in the TPS experiments (the H_2-consumption side of the TPS patterns is not shown in Fig. 7).

DISCUSSION

Reduction and Sulfidation Properties of Fe-exchanged Y-zeolite

The reduction of Fe-exchanged Y-zeolites, such as Fe–SK and Fe–LZY, can be considered to consist of two steps, leading to the α peak (low-temperature) and the β peak (high-temperature). From the quantitative TPR analysis of Fig. 2, the reduction pathway is presumed to proceed as $Fe^{3+} \rightarrow Fe^{2+}$ in the α peak and $Fe^{2+} \rightarrow Fe$ in the β peak. Applying this idea to the XRD results after TPR treatments (Fig. 3), it is concluded that the reduction of $Fe^{3+} \rightarrow Fe^{2+}$ proceeds without change of the zeolite framework structure. In contrast, the reduction of $Fe^{2+} \rightarrow Fe$ is always attended by complete destruction of the zeolite. The conservation of the zeolite framework structure in the reduction process of $Fe^{3+} \rightarrow Fe^{2+}$ is consistent with the view of reversible oxidation–reduction relationships between Fe^{2+}- and Fe^{3+}-exchanged Y-zeolites proposed by Boudart and co-workers (*7*, *8*). According to their estimation by Mössbauer spectroscopy, most of the Fe^{2+} ions of the dehydrated Fe^{2+}–Y (Si/Al = 3.0) are in the hexagonal prisms (S_I sites), and the others in fourfold coordination near the hexagonal window sites opening into the sodalite cages ($S_{I'}$) and the supercages ($S_{II'}$ and/or S_{II}) (*7–9*). The former and the latter Fe ions are bonded to six and three framework oxygen atoms, respectively. A crystallographic study of the distribution of Fe ions in Y-zeolite showed that the oxidation of Fe^{2+} to Fe^{3+} brings about a migration of the Fe ions of the hexagonal prisms (S_I sites) to the $S_{I'}$ sites (*9*). Accordingly, the $S_{I'}$ sites may be the sites of the Fe^{2+}-exchanged Y-zeolite (Fe^{2+}–Y), which was calcined to Fe^{3+}–Y and reduced again to Fe^{2+}–Y in the α peak in TPR. In any case, the Fe^{2+} ions in Fe^{2+}–Y can be expected to be stabilized in the zeolite pores and they cannot be reduced until the temperature is high enough that the zeolite framework commences to break down. The assignment of the β peak is confirmed by the apparent difference of the β peak temperature between Fe–SK (1154 K) and Fe–LZY (1298 K), because a zeolite of higher Si/Al framework exhibits a higher stability against hydrothermal treatment (*20*) and hence the stability of Fe–LZY

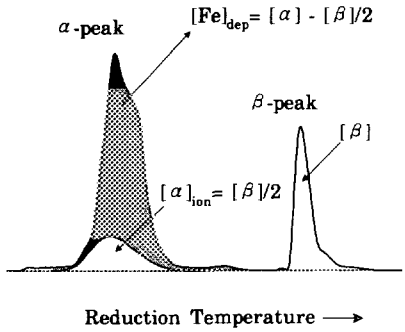

FIG. 8. Possible contribution of the ion-exchanged species and the aggregated ferric oxide to the TPR profile of Fe–LZY(A) in Fig. 2c.

(Si/Al = 4.8 by ^{29}Si NMR) is estimated to be much higher than that of Fe–SK (Si/Al = 2.6).

Another interpretation for the two reduction peaks may be a view that Fe^{3+} ions positioned at different sites in the zeolite are reduced at different temperatures. According to studies on Ni^{2+}-exchanged Y-zeolite (*21*), Ni^{2+} ions positioned at S_{II} and/or $S_{II'}$ sites were reduced at 793 K and those positioned at S_I sites at 1093 K. In the case of the Fe-exchanged Y-zeolite, however, this interpretation is excluded by the fact that the H_2-consumption ratios of the β and α peaks ($[\beta]/[\alpha]$) stay constant at 2.0 for both Fe–SK and Fe–LZY, which are considered to have different fractions of the cation sites accessible for Fe ions (*12, 13*).

The exceptionally small $[\beta]/[\alpha]$ ratio for Fe–LZY(A) can be accounted for by assuming that an additional reduction peak due to aggregated ferric oxide is superimposed on the α peak of the Fe-exchanged Y-zeolite. Figure 8 schematically shows the contributions of the ion-exchanged species and the aggregated ferric oxide to the TPR profile of Fe–LZY(A). According to the previous discussion, the real contribution for the reduction of ion-exchanged Fe^{3+} to Fe^{2+} should be equal to half the amount of H_2 consumed in the β peak ($[\alpha]_{ion} = [\beta]/2$). Assuming that the aggregated ferric oxide (or bulk Fe_2O_3) is reduced to metallic Fe and the Fe^{3+} to Fe^{2+} ions in the α peak, the amount of H_2 consumption for the aggregated ferric oxide ($[Fe]_{dep}$) can be determined as

$$[Fe]_{dep} = [\alpha] - [\beta]/2 \qquad (2)$$

with $[\alpha]$ and $[\beta]$ the amount of H_2 consumption in the α and β peaks, respectively. Applying Eq. (2) to the TPR of Fe–LZY(A), the H_2 consumption due to the reduction for the aggregated ferric oxide is estimated to be 66% of the total H_2 consumption.

Recently we reported the sulfidation mechanism of Co_3O_4 with varying crystallite size in connection with the catalytic activities of the resulting cobalt sulfides, as determined by means of TPS, XRD (*16*), and X-ray photoelectron spectroscopy (XPS) (*22*). The TPS patterns of bulk Fe_2O_3 used in this study seem comparable to those of the cobalt oxide calcined at 573 K [Co–O(573)], of which the sulfidation proceeds mainly via an O–S anion exchange followed by reduction of the lattice oxygen atoms (*16, 22*). As expected from the TPR reduction properties, the sulfidation of the Fe-exchanged Y-zeolite also proceeds in a quite different way as that of bulk Fe_2O_3. A large amount of H_2S is already consumed by adsorption on the Fe-exchanged Y-zeolite at 300 K. The adsorbed H_2S molecules are partly desorbed in peak I (380 K). As the sulfidation temperature is increased further, peak II (a set of an H_2S evolution and an H_2 consumption) appears without any preceding H_2S consumption and H_2 evolution at the lower temperature. Taking into account the fact that the previous TPS (sulfidation) treatment at 650 K as well as the TPR (reduction) treatment at 650 K bring about the disappearance of peak II in the second TPS measurement (Fig. 5b), the reaction occurring in peak II can not only be considered the hydrogenative desorption of sulfur [reaction (1)], but also the reduction of hydroxyl groups and/or oxygen atoms attached to Fe^{3+} ions, resulting in the reduction of the Fe^{3+}-exchanged Y-zeolite (Fe^{3+}–Y) to the Fe^{2+}-exchanged Y-zeolite (Fe^{2+}–Y). By

considering the presence of $Fe^{3+}-O^{2-}-Fe^{3+}$ bridges located inside the sodalite cage in the dehydrated $Fe^{3+}-Y$ (*8*), the reaction of the Fe-exchanged Y-zeolite during the TPS up to peak II may be described as follows:

Oxidation at room temperature (300 K)

$$2\,Fe^{2+}(*) + \tfrac{1}{2}\,O_2 + H_2O \rightleftharpoons 2\,Fe^{3+}(OH)^-(*) \quad (3)$$

(dehydrated $Fe^{2+}-Y$) (hydrated $Fe^{3+}-Y$)

Calcination at 650 K

$$2\,Fe^{2+}(*) \text{ or } 2\,Fe^{3+}(OH)^-(*) \xrightarrow{+\,O_2} Fe^{3+}-O^{2-}-Fe^{3+}(*) + H_2O \quad (4)$$

(dehydrated $Fe^{3+}-Y$)

TPS (sulfidation) treatment up to peak II at 300 K

$$Fe^{3+}-O^{2-}-Fe^{3+}(*) + H_2S \rightarrow Fe^{3+}(OH)^-(*) + Fe^{3+}(SH)^-(*) \quad (5\text{-}1)$$

or

$$Fe^{3+}-O^{2-}-Fe^{3+}(*) + H_2S \rightarrow Fe^{3+}-S^{2-}-Fe^{3+}(*) + H_2O \quad (6\text{-}1)$$

in peak II

$$Fe^{3+}(OH)^-(*) + \tfrac{1}{2}\,H_2 \rightarrow Fe^{2+}(*) + H_2O \quad (5\text{-}2)$$

(dehydrated $Fe^{2+}-Y$)

and

$$Fe^{3+}(SH)^-(*) + \tfrac{1}{2}\,H^2 \rightarrow Fe^{2+}(*) + H_2S \quad (5\text{-}3)$$

or

$$Fe^{3+}-S^{2-}-Fe^{3+}(*) + H^2 \rightarrow 2\,Fe^{2+}(*) + H_2S. \quad (6\text{-}2)$$

The symbol (*) refers to the species situated at some ion-exchanged sites in the zeolite. The existence of either the hydrogensulfide anion species $Fe^{3+}(SH)^-$ or the $Fe^{3+}-S^{2-}-Fe^{3+}$ bridge species during the sulfidation process in $Fe^{3+}-Y$ has not been established in this study. Nevertheless, the TPS treatment up to peak II may be regarded to have the same effect as the TPR treatment up to the α peak, in view of the fact that the dehydrated $Fe^{2+}-Y$ is produced in either treatment.

Peak III, a steep H_2S-consumption peak at the higher temperature in TPS, can be compared with the β peak in TPR from the standpoint of the zeolite framework destruction as a limiting-step of both reactions, although peak III involves the sulfidation reaction of $Fe^{2+}-Y$ probably to FeS and the β peak represents reduction to metallic Fe. After the sulfidation in peak II, the resulting dehydrated $Fe^{2+}-Y$, in which the Fe^{2+} ion is still bonded to some framework oxygen atoms, is too stable to be subjected to further reduction and/or sulfidation until the temperature emerging peak III. Once the framework of the zeolite begins to decompose at a sufficiently high temperature, the Fe^{2+} ion can easily be sulfided to FeS as

$$Fe^{2+}(*) + H_2S \rightarrow FeS + H_2O \quad (7)$$

(dehydrated $Fe^{2+}-Y$)

or a combination of the following reactions:

$$Fe^{2+}(*) + H_2 \rightarrow Fe^0 + H_2O \quad (8\text{-}1)$$

$$Fe^0 + H_2S \rightarrow FeS + H_2. \quad (8\text{-}2)$$

One question still remains why a temperature difference between peak III and the β peak exists of +71 K (1225–1154 K) for Fe–SK and +12 K (1310–1298 K) for Fe–LZY. There might be a different thermal stability of the Fe-containing Y-zeolite in the presence of H_2S/H_2 mixtures and pure H_2.

Reduction and Sulfidation Properties of Fe-treated Y-zeolite

At the first stage of the preparation, it is evident from the TPR in Fig. 6 and TPS in Fig. 7 that the Fe-species in Fe/LZY(b) can be regarded to be the same as those in the Fe-exchanged Y-zeolite (Fe-LZY). On the other hand, the low-temperature shifts of the β peaks in TPR in the process of the Fe-

treatment (Fig. 6) suggest a structural or site change of the Fe-species, which make them easier to reduce than those in the Fe-exchanged Y-zeolite. The decrease in the number of ion-exchanged species with the treatment is identified by comparing the intensities of peak III in Fig. 7, which is assigned to the sulfidation of the Fe^{2+} ions at the ion-exchanged sites to FeS as described in reaction (7), or (8-1) and (8-2). Peak III decreases significantly in intensity from Fe/LZY(b) to Fe/LZY(h). The increase of the broad H_2S-consumption peaks at 800–1200 K at the expense of peak III in TPS also indicates that the Fe-species at the ion-exchanged sites are transformed into a new state which is easier to sulfide. For this H_2S-consumption peak, the change of the sulfidation property by proceeding the Fe-treatment is more significant than that of the reduction property (the β peaks in TPR). This indicates that the sulfidation of the Fe-species in the Fe-treated Y-zeolite becomes easier than the reduction. One possible explanation for the ease of sulfidation may be a strong attraction ability of the Fe-species to H_2S. It may well be that H_2S effectively weakens the interaction between some kind of Fe-species and the framework oxygen atoms. After all, the results of both TPR and TPS data suggest that the Fe-species in the Fe-treated Y-zeolite are first introduced in the zeolite pores as the ion-exchanged species, and become more reactive under both reduction and sulfidation on proceeding the Fe-treatment.

There are at least two possible explanations for the changes in the state of the Fe-species in the zeolite. One is the migration of Fe ions from inside the sodalite cages and/or hexagonal prisms to inside the supercages. The Fe-oxide species inside the supercages are considered to facilitate the reduction and the sulfidation because of a smaller size restriction. This idea was proposed by Suzuki and co-workers for Ni^{2+}-exchanged Y-zeolite, the Ni^{2+} ions in which were supposed to migrate from inside the sodalite cages to inside the supercages by treatment with an aqueous NaOH above pH 10.8 (*21, 23*). The other is a decreasing interaction between the Fe-species and the framework oxygen atoms. This situation can be expected to occur when the Fe-oxide clusters such as di- or polynuclear μ^2-oxo-iron complexes are formed by hydrolysis of Fe ions followed by calcination. The formation of the small Fe-oxide clusters was corroborated by the EXAFS (extended X-ray absorption fine structure) analysis for the same series of the Fe-treated Y-zeolites, in which it was found that the contribution of the Fe atoms with second-nearest Fe neighbors was apparently enlarged on proceeding the Fe-treatment (*24*). On the other hand, the invariance of the α peak and $[\beta]/[\alpha]$ ratio at 2.0 in TPR during the treatment indicate that the stabilization of the Fe^{2+} ions against reduction is maintained to some extent even though the reduction of the Fe^{2+}-species (β peak) shifts to lower temperature. Thus the resulting Fe-oxide clusters are still stabilized through a coordination with the framework oxygen atoms. In contrast to the constant peak position of the α peak in TPR, peak II in TPS shifts to lower temperature on proceeding the Fe-treatment. The ease of reduction of the Fe^{3+}- to Fe^{2+}-species in peak II (TPS) compare with that in the α peak (TPR) may be due to the stronger reducing ability of H_2S/H_2 mixtures than that of pure H_2 (*25*). One can conclude that the sulfidation of Fe-oxide species by an H_2S/H_2 mixture is more structural sensitive than the reduction by H_2. It is interesting to determine the exact position and the detailed structure of the Fe-oxide clusters in Y-zeolite. However, on the basis of the present data alone it can not be discussed in further detail.

The prolonged Fe-treatment of the zeolite suspension causes substantial changes on both the TPR and TPS patterns of Fe/LZY(i). Although the β peak in the TPR of Fe/LZY(i) seems to shift continuously to lower temperature with the treatment, the α' peak around 890 K appears abruptly after the broad α peak around 600 K (Fig. 6i).

Concurrently, the twin H_2S-evolution peaks (with the twin H_2-consumption peaks) appear in place of the single peak II in TPS (Fig. 7i). It is conceivable that an oligomerization of the small Fe-oxide clusters proceeds with the prolonged Fe-treatment and that small Fe-oxide species are formed with much weaker interaction to the framework oxygen atoms (probably still situated inside the supercages). The reduction of such species can be much easier than that with coordination to the framework oxygen atoms, and thus assigned to the α' peak in TPR. Additionally, the Fe-oxide species reduced at the α' peak may be distinguished for the reduction temperature from the aggregated ferric oxides on the external surface of the zeolite, which are observed for Fe–LZY(A) and reduced at 724 K in TPR.

In spite of the slight modification of the TPR pattern of Fe/LZY(i), there is a pronounced variation in the shape of the TPS. It is proposed that minor iron species can play an important role in changing the whole sulfidation process. As can be seen in the TPS of MoO_3/Al_2O_3 (*18*), CrO_3/Al_2O_3 (*19*), CoO/Al_2O_3 (*26*), and CoO/SiO_2 (*16, 22, 25*), sulfidation of highly dispersed oxides on support (small Fe-oxide species) occurs at much lower temperature than that of bulk oxide (crystalline Fe_2O_3), mainly since H_2S is not limited by diffusion (*16, 25*). The sulfidation of the Fe-oxide species, which are reduced in the α' peak in TPR, thus can be attributed to the H_2S-consumption peak at 415 K, and may form FeS_{1+x} in this temperature range. The resulting FeS_{1+x} is partially reduced at higher temperature to form a more stable sulfide, $FeS_{1+x'}$ $(0 \leq x' < x)$, according to the following reaction:

$$FeS_{1+x} + (x - x')\,H_2 \rightarrow FeS_{1+x'} + (x - x')\,H_2S. \quad (9)$$

This hydrogenative desorption of the sulfur should be attributed to the smaller peak at the higher temperature side of the twin peaks (at 557 K), since such easily sulfidable Fe-oxide species is regarded as a minor compound. The remaining bigger peak at the lower-temperature side of the twin peaks (at 497 K) is accordingly assigned to the same peak II as that of Fe/LZY(b)–(h) (at 627–584 K). The low-temperature shift of 87 K for peak II of Fe/LZY(i) compared with that of Fe/LZY(h) cannot be explained only on the structural change of the Fe-oxide clusters, because the previous temperature difference of peak II between Fe/LZY(h) and Fe/LZY(b) is observed only 43 K. A possible explanation for the unexpectedly low-temperature shift may be the accelerative reduction of sulfur atoms catalyzed by FeS_{1+x} formed mainly at 417 K. Similar phenomena were reported in case of the sulfidation of Co promoted MoO_3/Al_2O_3 by TPS (*27*), and the reduction of unsupported FeMo, CoMo, and NiMo sulfide catalysts by temperature-programmed sulfur extraction (*28*). In all cases, the promoter atom plays a role in increasing the reducibility of the sulfided-Mo precursor. It may be concluded that the twin hydrogenative H_2S-desorption peaks in TPS indicate the presence of at least two different kinds of Fe-oxide species inside the zeolite pores from the point of view of the interaction to the framework oxygen atoms. This idea is confirmed by comparing the TPS patterns of the various kinds of Fe-treated Y-zeolites with the estimated H_2-consumption for the aggregated ferric oxide obtained from the TPR data, which should involve the contribution of the α' peak. It is shown in Fig. 9 that the twin hydrogenative H_2S-desorption peaks in TPS appear whenever aggregated ferric oxide is present.

Taking into account the above considerations, a plausible interpretation of the TPR and TPS results for the Fe-treated Y-zeolites is schematically presented in Fig. 10. Judged by the presence of peak III as a strong H_2S consumption in TPS, ion-exchanged species can be identified as the dominant species at the first stage of the Fe-treatment. The second-appearing dominant species, which is supposed to be the small Fe-oxide clusters located inside the supercages with strong interaction to the frame-

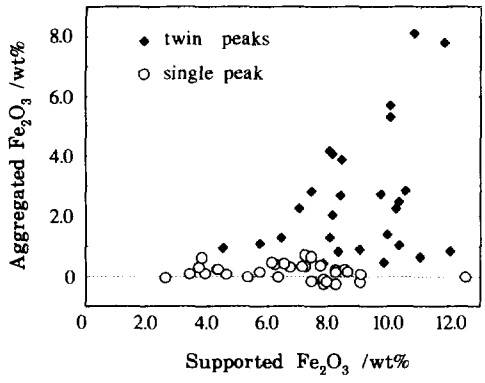

FIG. 9. The estimated amount of the aggregated ferric oxide obtained from the H_2-consumption of the TPR data by using Eq. (2) in text versus the amount of supported iron as Fe_2O_3 in the various kinds of Fe-treated Y-zeolites. The symbols open circle and filled diamond indicate that the sample shows single and twin peak-II's in TPS, respectively.

work oxygen atoms, appears in the place of the ion-exchanged species when the heat-treatment is applied. This transformation can be confirmed by evaluating the lower temperature shifts of either the β peak in TPR or peak II in TPS, as well as the decrease in intensity of peak III. Finally, Fe oxide without interaction to the zeolite framework oxygen atoms is produced and this leads to the aggregated ferric oxide by the redundant Fe-treatment. The presence of these species is clearly discernible from the existence of the twin peak II in TPS, and the amount is evaluated from the H_2 consumptions of the α and β peaks in TPR. Accordingly by combining the TPR and TPS data, we can differentiate between three major types of Fe-oxide species in and/or on the zeolite.

Activity for Toluene Disproportionation

The activity of the Fe-treated Y-zeolites for toluene disproportionation increases dramatically by applying the heat-treatment up to 323 K [Fe/LZY(b)–(e)], suggesting that new acidic properties are generated in the presence of H_2S (*2*). This increase in activity apparently coincides with the formation of the small Fe-oxide clusters (inside the supercages) at the expense of the ion-exchanged species, as shown in Fig. 10. Although the mechanism for generating the new acidic sites is still obscure, it can be presumed that toluene molecules cannot approach the ion-exchanged species even inside the sodalite cages as well as that inside the hexagonal prisms. The high activity can be accounted for by the formation of small Fe-oxide clusters inside the supercages. From comparisons of TPR and TPS results, it is evident that these Fe-species are still coordination to the framework oxygen atoms to stabilize the oxidic state (probably Fe^{2+}) under both reductive (TPR) and sulfidic (TPS) conditions. It might be presumed that the stabilization of the oxidic state holds

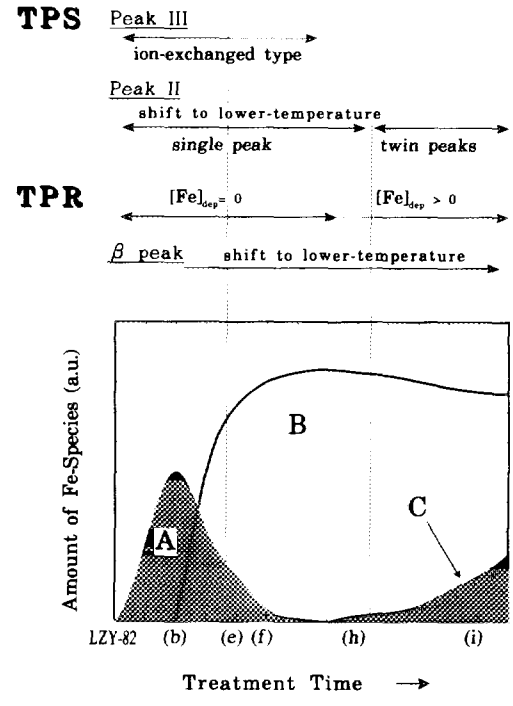

FIG. 10. Possible Fe-species distribution estimated from TPR and TPS results against the treatment time for the Fe-treated Y-zeolites: (A) ion-exchanged species, (B) Fe-oxide clusters inside the supercages with strong interaction to the framework oxygen atoms, and (C) Fe oxide without interaction to the zeolite (including the aggregated ferric oxide).

even under the reaction conditions (0.2 vol% H_2S/H_2, 6 MPa at 623 K). Iino and co-workers have proposed that the adsorption of H_2S on such oxidic Fe-species accounts for the generation of the unique acidity required to catalyze the hydrocracking reaction as well as the toluene disproportionation (*1, 2, 6*).

On proceeding the Fe-treatment, the interaction between the Fe-species and the framework oxygen atoms is weakened by hydrolysis and eventually the Fe oxides aggregate to form the bulk ferric oxide. From the standpoint of the production control, it is desirable that the Fe-treated Y-zeolite should be taken out at a time when the amount of the small Fe-oxide clusters inside the supercages reaches its maximum, and when the amount of the aggregated ferric oxide is still at a minimum, as shown in Fig. 10. Judged from the activity maximum, the most active species may be attributed to the small Fe-oxide clusters just modified from the ion-exchanged species. It should be pointed out that both the β peak (TPR) and peak II (TPS) steadily shift to lower temperatures as long as the Fe-treatment is continued. A more exact production control for the active catalyst might be feasible by determining the optimum temperature of the β peak and/or peak II.

It should be also noted that zeolite-related acid sites must be considered to account for the actual activity. For instance, it has been established that an extralattice aluminum species of steam dealuminated Y-zeolites (*29*) as well as the framework aluminum (*30, 31*) strongly affects the acidity of a zeolite catalyst. Taking our results consideration, however, the active Fe-species is likely to account for a large part of the activity in our catalysis system.

CONCLUSIONS

Reduction and sulfidation properties of a series of Fe-treated Y-zeolites as well as Fe-exchanged Y-zeolites are investigated by TPR and TPS. As the Fe^{2+}-species in the Fe-exchanged Y-zeolite are stabilized inside the sodalite cages and/or the hexagonal prisms, both reduction and sulfidation of the Fe^{2+}-species are difficult until the temperature is high enough that the zeolite framework commences to break down, in contrast to the easy reduction of the Fe^{3+}- to Fe^{2+}-species. The aggregated ferric oxide deposited on the zeolite surface can be quantitatively distinguished from the ion-exchanged type species by evaluating the TPR profile.

At the first stage of the preparation of the Fe-treated Y-zeolite, the Fe-species are introduced in the zeolite in the ion-exchanged form. In the process of the Fe-treatment, the Fe-species adopt the new structures and become more reactive under both reduction and sulfidation. This is accounted for by the formation of small Fe-oxide clusters inside the supercages, which are still coordination to the framework oxygen atoms, and exhibit a high activity for toluene disproportionation in the presence of H_2S. A prolonged heat-treatment causes the oligomerization of the Fe-oxide clusters because of a lowering of the interaction with the zeolite, and the aggregation of the Fe oxides to bulk ferric oxide.

These changes of the Fe-species in the zeolite can be clarified and quantified by combining TPR and TPS techniques, as shown in Fig. 10.

ACKNOWLEDGMENTS

We gratefully acknowledge Professor J. A. Moulijn (Delft University of Technology) and Dr. P. J. Mangnus for providing the opportunity to measure some samples with their TPS instrument at the University of Amsterdam in 1987, which motivated us to initiate this study. One of the authors (K.I.) thanks Professor R. Prins (Swiss Federal Institute of Technology, Zürich) for helpful discussions.

REFERENCES

1. Iino, A., Iwamoto, R., and Nakamura, I., "Catalytic Science and Technology," Vol. 1, p. 351. Kodansha, Tokyo, 1991.
2. Hidaka, S., Iino, A., Gotoh, M., Ishikawa, N., Mibuchi, T., and Nita, K., *Appl. Catal.* **43,** 57 (1988).
3. Iwamoto, R., Nita, K., Hidaka, S., Inamura, K., and Iino, A., *in* "Acid–Base Catalysis" (K. Tanabe *et al.*, Eds.), p. 313. Kodansha, Tokyo, 1989.

4. Hidaka, S., Iino, A., Mibuchi, T., Nita, K., and Yamazoe, N., *Chem. Lett.*, 1213 (1986).
5. Hidaka, S., Iino, A., Mibuchi, T., Nita, K., Maeda, Y., and Yamazoe, N., *J. Chem. Soc. Jpn.* **9,** 1659 (1987).
6. Hidaka, S., Iino, A., Nita, K., Morinaga, K., and Yamazoe, N., *Bull. Chem. Soc. Jpn.* **61,** 3169 (1988).
7. Delgass, W. N., Garten, R. L., and Boudart, M., *J. Phys. Chem.* **73,** 2970 (1969).
8. Garten, R. L., Delgass, W. N., and Boudart, M., *J. Catal.* **18,** 90 (1970).
9. Pearce, J. R., Mortier, W. J., and Uytterhoeven, J. B., *J. Chem. Soc. Faraday Trans. I* **77,** 937 (1981).
10. Fu, C. M., Korchak, V. N., and Hall, W. K., *J. Catal.* **68,** 166 (1981).
11. Leglise, J., Petunchi, J. O., and Hall, W. K., *J. Catal.* **86,** 392 (1984).
12. Aparicio, L. M., Dumesic, J. A., Fang, S.-M., Long, M. A., Ulla, M. A., Millman, W. S., and Hall, W. K., *J. Catal.* **104,** 381 (1987).
13. Schmidt, R., Amiridis, M. D., Dumesic, J. A., Zelewski, L. M., and Millman, W. S., *J. Phys. Chem.* **96,** 8142 (1992).
14. Melchior, M. T., Vaughan, D. E. W., and Jacobson, A. J., *J. Am. Chem. Soc.* **104,** 4859 (1982).
15. Inamura, K., *Shokubai* (Catalysis Society of Japan) **33,** 356 (1991).
16. Inamura, K., Takyu, T., Okamoto, Y., Nagata, K., and Imanaka, T., *J. Catal.* **133,** 498 (1992).
17. Wimmers, O. J., Arnoldy, P., and Moulijn, J. A., *J. Phys. Chem.* **90,** 1331 (1986).
18. Arnoldy, P., van den Heijkant, J. A. M., de Bok, G. D., and Moulijn, J. A., *J. Catal.* **92,** 35 (1985).
19. Mangnus, P. J., Ellison, A., Scheffer, B., and Moulijn, J. A., *Bull. Soc. Chim. Belg.* **96,** 977 (1987).
20. Venuto, P. B., "Molecular Sieve Zeolite." Adv. Chem. Ser., Vol. 102. Am. Chem. Soc., Washington, DC, 1971.
21. Suzuki, M., Tsutsumi, K., Takahashi, H., and Saito, Y., *Zeolites* **8,** 284 (1988).
22. Okamoto, Y., Nagata, K., Imanaka, T., Inamura, K., and Takyu, T., *Bull. Chem. Soc. Jpn.* **65,** 1331 (1992).
23. Sano, M., Maruo, T., Yamatera, H., Suzuki, M., and Saito, Y., *J. Am. Chem. Soc.* **109**(1), 52 (1987).
24. Inamura, K., *et al.*, unpublished work.
25. Castner, D. G., and Watson, P. R., *J. Phys. Chem.* **95,** 6617 (1991).
26. Arnoldy, P., de Booys, J. L., Scheffer, B., and Moulijn, J. A., *J. Catal.* **96,** 122 (1985).
27. Scheffer, B., de Jonge, J. C. M., Arnoldy, P., and Moulijn, J. A., *Bull. Soc. Chim. Belg.* **93,** 751 (1984).
28. Göbölös, S., Wu, Q., Andre', O., Delannay, F., and Delmon, B., *J. Chem. Soc. Faraday Trans. I* **82,** 2423 (1986).
29. Shertukde, P. V., Hall, W. K., and Marcelin, G., *Catal. Today* **15,** 491 (1992).
30. Fleisch, T. H., Meyers, B. L., Ray, G. J., Hall, J. B., and Marshall, C. L., *J. Catal.* **99,** 117 (1986).
31. Bezman, R., *Catal. Today* **13,** 143 (1992).